The Dependence on the Moho Depth of the *b*-Value of the Gutenberg–Richter Law

Cataldo Godano*[1,2], Anna Tramelli[2], Giuseppe Petrillo[1], Eliana Bellucci Sessa[2], and Eugenio Lippiello[1]

ABSTRACT

We investigate the dependence of the Gutenberg–Richter *b* parameter on the crustal thickness quantified by the Moho depth, for nine different regional catalogs. We find that, for all the catalogs considered in our study, the *b*-value is larger in areas presenting a thicker crust. This result appears in apparent contradiction with previous findings of a *b* decreasing with the focal depth. However, both the results are consistent with acoustic emission experiments, indicating a *b*-value inversely proportion to the applied differential stress. Our results can be indeed interpreted as the signature of a larger stress concentration in areas presenting a thinner crust. This is compatible with the scenario where postseismic deformation plays a central role in stress concentration and in aftershock triggering.

KEY POINTS

- We examine the relationship between Gutenberg–Richter *b*-values and crustal thickness, as defined by Moho depth.
- We find *b*-values to be larger in areas of thicker crust, due to less stress concentration than in thin crust.
- Results show the importance of postseismic deformation in stress concentration and aftershock triggering.

INTRODUCTION

The Gutenberg–Richter (GR) law states that earthquake magnitudes are exponentially distributed (Gutenberg and Richter, 1944) as $\mathrm{Log}_{10}N = a - bm$, in which N is the number of earthquakes with magnitude larger or equal to m, b is a scaling parameter, and a is a constant. Analysis of instrumental catalogs usually reveal that b assumes values very close to 1, quite independently of the considered geographic region and time window. This suggests that the b-value for tectonic earthquakes does not differ significantly from a common universal value. On the other hand, the size distribution of acoustic emissions from microfracturing in rock fracture experiments, which is consistent with the GR law, indicates a b-value that linearly decreases by increasing the differential stress (Scholz, 1968; Amitrano, 2003). Extending this observation to tectonic earthquakes is a very difficult task. Indeed, the magnitude–frequency distribution can be altered by several factors such as short-term aftershock incompleteness (Kagan, 2004; Helmstetter *et al.*, 2006; Enescu *et al.*, 2007; Peng *et al.*, 2007; Hainzl, 2016a,b; Lippiello *et al.*, 2017; de Arcangelis *et al.*, 2018; Lippiello, Cirillo, *et al.*, 2019; Lippiello, Godano, and de Arcangelis, 2019), artificial changes in the reporting of magnitudes (Thormann *et al.*, 2010; Kamer and Hiemer, 2015), mixing of different magnitude definitions (Kanamori, 1983), and so forth. These factors can introduce strong biases in the estimate of the b-value, and it is, therefore, always very difficult to discriminate between genuine b changes from spurious fluctuations. These problems are present also using high-resolution catalogs (Herrmann and Marzocchi, 2021). Nevertheless, several results provide an indirect support to the hypothesis of an inverse stress dependence of the b-values, also for tectonic earthquakes. It has been indeed found that the b-value for earthquakes in the continental crust decreases approximately linear with depth (Mori and Abercrombie, 1997; Spada *et al.*, 2013; Scholz, 2015). Furthermore, a clear dependence of the b-value on earthquake focal mechanism has been documented, with the b-value being smaller for thrust than for normal-faulting events and having an intermediate value for strike-slip earthquakes (Schorlemmer *et al.*, 2005; Gulia and Wiemer, 2010; Petruccelli *et al.*, 2018). Recently, a unifying empirical framework is proposed to link the b-value with Anderson's faulting theory and differential stress (Petruccelli, Schorlemmer, *et al.*, 2019).

In this study, we evaluate the b-value in regions presenting a different depth ζ of the Mohorovičić discontinuity, or Moho in abbreviated form, which separates crust from the underlying upper mantle. Under the assumption of an inverse dependence

1. Department of Mathematics and Physics, Università della Campania Luigi Vanvitelli, Caserta, Italy, https://orcid.org/0000-0003-1444-1889 (EL); 2. Istituto Nazionale di Geofisica e Vulcanologia, Sezione di Napoli Osservatorio Vesuviano, Naples, Italy, https://orcid.org/0000-0001-6259-5730 (AT); https://orcid.org/0000-0003-2521-6476 (EBS)

*Corresponding author: cataldo.godano@unicampania.it

Cite this article as Godano, C., A. Tramelli, G. Petrillo, E. Bellucci Sessa, and E. Lippiello (2022). The Dependence on the Moho Depth of the *b*-Value of the Gutenberg–Richter Law, *Bull. Seismol. Soc. Am.* **112**, 1921–1934, doi: 10.1785/0120210144

TABLE 1
The Areas, the Institutions (the Names of the Institutions Not in Acronym Can Be Found in the Acknowledgments) That Make Available the Earthquake Catalogs and the Websites from Where the Earthquake Catalogs Can Be Downloaded

Area	Institution	Website
Arabia	ISC	http://www.isc.ac.uk/iscbulletin/search/bulletin/
Canada–Alaska	ISC	http://www.isc.ac.uk/iscbulletin/search/bulletin/
Japan	JMA	data.jma.go.jp/svd/eqev/data/bulletin/index_e.html
Italy	INGV	cnt.rm.ingv.it
North California	NCEDC	ncedc.org/ncedc catalogsearch.html
Fennoscandia	ISC	http://www.isc.ac.uk/iscbulletin/search/bulletin/
South California	SCEDC	scedc.caltech.edu/data/alt-2011-dd-hauksson-yang-shearer.html
South California	Foc. Mech.	scedc.caltech.edu/data/alt-2011-yang-hauksson-shearer.html
United States–California	ISC	http://www.isc.ac.uk/iscbulletin/search/bulletin/
Tibet and China	ISC	http://www.isc.ac.uk/iscbulletin/search/bulletin/

The South California catalog is the relocated one (Hauksson *et al.*, 2012). United States–California stays for United States and Central America. INGV, Istituto Nazionale di Geofisica e Vulcanologia; ISC, International Seismological Centre; JMA, Japan Meteorological Agency; NCEDC, Northern California Earthquake Data Center; and SCEDC, Southern California Earthquake Data Center.

of the *b*-value on the differential stress, our analysis can provide a connection between the level of stress concentration and the thickness of the crust. This study must not be confused with the already mentioned (Mori and Abercrombie, 1997; Spada *et al.*, 2013; Scholz, 2015) existing results about the *b*-value dependence on the earthquake focal depth, which is not directly related to ζ. Indeed, if a small ζ imposes an upper bound on the maximum focal depth, it is common to find shallow earthquakes also in regions presenting a very large ζ. Here, we present results for magnitude–frequency distribution in different geographic regions of the world, which have been selected according to the following criteria: (1) the existence of a seismic catalog with an homogeneous definition of the magnitude, extending over the whole region; (2) the availability of maps with an accurate location of the Moho depth ζ; (3) a deviation from the mean of the ζ-value over the region, which must be larger than 50% of the mean regional ζ-value. Only nine regions in the world (see Table 1) satisfy all the three criteria and are presented in the following section where also the adopted methodology is discussed. Results are presented in the subsequent section, and a possible interpretation of the physical mechanisms responsible for their occurrence can be found in the Discussion section. Conclusions are finally drawn in the last section.

DATA AND METHOD

The position of the Moho discontinuity has been deeply investigated in different seismogenic regions. We have focused our study on nine different areas of the world where a sufficiently good quality map of the Moho depth ζ is produced. More precisely, we choose those regions presenting a sufficiently wide interval of ζ, which allows us to perform accurate statistical tests. The map of ζ inside each area is plotted in Figure 1.

The nine areas are listed in Table 1, whereas in Table 2 we report the temporal periods here analyzed for the different catalogs, and in Table 3 we report the references of the studies in which the Moho depth maps, used in our analysis, have been produced. For each of the nine selected areas, we have considered the best-available regional seismic catalog. The institutions and the websites that make available the earthquake catalogs here analyzed are reported in Table 1. Using catalogs of South California, North California, and United States–California leads to some overlap between the three catalogs. However, the overlap is very small (less than 10%) and does not significantly affect our results. We remark that the revised (Storchak *et al.*, 2017, 2020) International Seismological Centre (ISC) catalog reports different magnitudes for the same earthquake. A smaller overlap does exist also at the border between the Canada–Alaska and the United States–California regions. Even, in this case, the overlap does not affects our results. In this study, we choose the magnitude according to the order of preference suggested by Di Giacomo and Storchak (2016): (1) M_w, (2) M_s, (3) m_b, and (4) m_L, respectively.

Each map has been georeferenced, vectorized, and, in this way, by means of an interpolation via ArcGIS tools (GIS, 2011), we have been able to associate to each earthquake in a regional catalog the value of the Moho depth ζ beneath its epicentral coordinate. This implies that each earthquake i in the catalog is characterized by its magnitude m_i, occurrence time t_i, hypocentral coordinates x_i, y_i, z_i, and the Moho depth ζ_i beneath its location. This procedure provides us the value of ζ_i with a resolution of about 0.1°, in latitude and longitude, inside the nine considered regions. The value of ζ_i used in our study is in substantial agreement with the results obtained in more recent studies (Bagherbandi *et al.*, 2015; Szwillus *et al.*, 2019; Abrehdary and Sjöberg, 2021) with differences that are comparable with the typical uncertainty in the Moho evaluation. In particular, a global map of Moho depth in the crystalline crust, together with the interpolation error and error covariance, has been recently obtained by Szwillus *et al.*

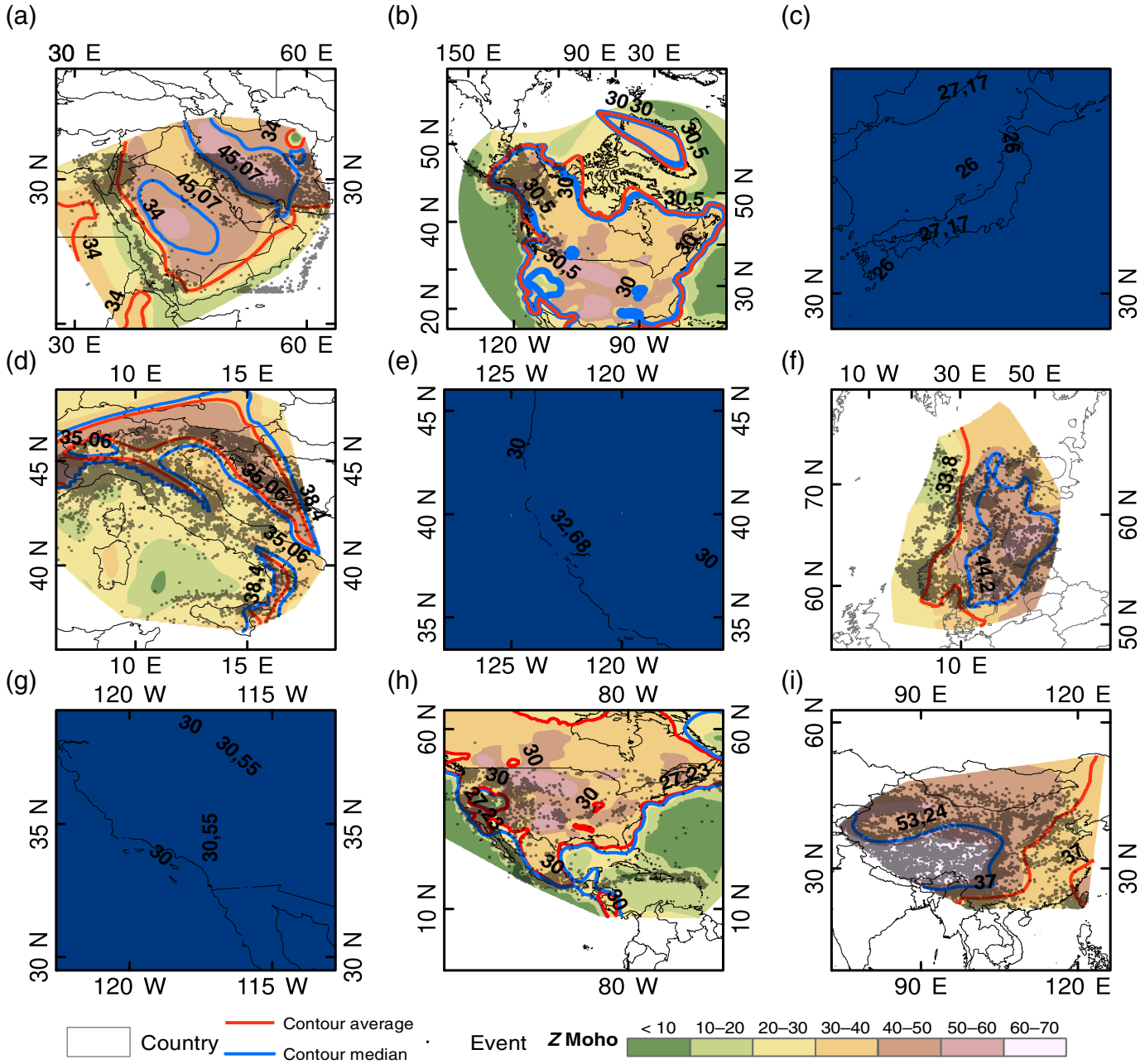

(2019). This study, however, provides the value of ζ_i with a resolution of 1° in latitude and longitude, which is too low for the purposes of our study.

We have excluded by our analysis all the earthquakes with $z_i > \zeta_i$, namely all earthquakes occurring beneath the Moho. The latter choice avoids difficulties in the interpretation of results in subduction zones. In general, the percentage of neglected events is so small in each catalog (in the range 0%÷6.0%) that no significant change could be found if also earthquakes with $z_i > \zeta_i$ are included. The only exception is represented by the Japan where differences are found and are related to the presence of the subducting slab.

Different regional catalogs can implement a different definition of the magnitude and, at the same time, can present important differences in the value of the completeness magnitude. The estimate of b is strongly affected by the previous two features, and it is, therefore, not possible to make a quantitative comparison between the b-values obtained in two different regional catalogs. We, therefore, investigate the dependence

Figure 1. The map of the Moho depth for the nine considered geographic areas. (a) Arabia, (b) Canada–Alaska, (c) Japan, (d) Italy, (e) Northern California, (f) Fennoscandia, (g) Southern California, (h) United States–California, and (i) Tibet and China. The value of ζ can be read from the color bar code. Black points indicate the epicentral coordinates of the earthquakes present in the regional seismic catalogs. The red and blue contours represent the average Moho depth ζ_a and its median value ζ_m, respectively. The color version of this figure is available only in the electronic edition.

TABLE 2
The Temporal Periods of the Catalogs Analyzed Here

Regions	Start Date (yyyy/mm/dd)	End Date (yyyy/mm/dd)
Arabia	1979/01/05	2019/10/31
Canada–Alaska	1979/01/04	2019/10/31
Japan	1998/01/01	2017/12/31
Italy	2003/01/01	2019/12/31
North California	1985/01/01	2018/12/31
Fennoscandia	1979/01/10	2019/10/31
South California	1981/01/01	2018/12/31
South California (Foc. Mech)	1981/01/01	2019/12/31
United States–California	1979/01/01	2019/10/31
Tibet and China	1979/01/01	2019/10/31

of the b-value as function of ζ inside each regional catalog. In particular, inside each regional catalog, we group earthquakes into two separated classes: Class A includes those earthquakes occurring inside areas with a thinner crust, that is, earthquakes with the Moho depth ζ_i beneath its location smaller than a reference value $\overline{\zeta}$, $\text{zeta}_i < \overline{\zeta}$. Class B, conversely, includes those earthquakes occurring inside areas with a thicker crust, that is, $\text{zeta}_i \geq \overline{\zeta}$. We consider two choices for the discriminating threshold $\overline{\zeta}$: (1) the average depth of the Moho $\overline{\zeta} = \zeta_a = (\zeta_{\max} + \zeta_{\min})/2$ (in which $\zeta_{\min}$ and $\zeta_{\max}$ represent the minimum and the maximum value of the Moho depth in the considered region, respectively), (2) the median of the Moho depth $\overline{\zeta} = \zeta_m$, namely the value of $\overline{\zeta}$, separates the whole population of N earthquakes into two subsets, each one containing exactly $N/2$ earthquakes. The values of $\zeta_{\min}$, $\zeta_{\max}$, and ζ_m are listed in Table 4 for each of the nine considered regions. The location depth z_i of an earthquake does not influence the belonging to a given class, except if that earthquake occurs below the Moho and is, therefore, not considered in the study. As an example, in the Canada–Alaska area $\zeta_a = 35$ km and an earthquake with $z_i = 30$ km belongs to class A if the Moho depth ζ_i beneath its epicenter is smaller than 35 km. Conversely, an earthquake occurring at a depth of $z_i = 5$ km, with an epicentral location in a region such as the local Moho depth $\zeta_i = 40$ km, belongs to class B.

TABLE 3
The Regions and the Reference of the Articles from Where We Have Extracted the Moho Maps

Regions	References
Arabia	Baranov (2010)
Canada–Alaska	Mooney and Kaban (2010)
Japan	Katsumata (2010)
Italy	Piana Agostinetti and Amato (2009)
North California	Mooney and Kaban (2010)
Fennoscandia	Bannister *et al.* (1991)
South California	Mooney and Kaban (2010)
United States–California	Mooney and Kaban (2010)
Tibet and China	Baranov (2010)

TABLE 4
The $\zeta_{\min}$ and $\zeta_{\max}$ Values for the Different Geographic Regions

Area	$\zeta_{\min}$	$\zeta_{\max}$	ζ_m
Arabia	12	56	45.07
Canada–Alaska	10	60	30.5
Japan	14	38	27.17
Italy	14	63	35.06
North California	10	50	32.68
Fennoscandia	18	56	44.2
South California	10	50	30.55
United States–California	2	60	27.23
Tibet and China	30	74	53.24

RESULTS

For each regional catalog, we separately evaluate the magnitude distribution $N(m)$ inside each of the two classes. The completeness magnitude m_c is then estimated using three different methods: the maximum curvature method (MCM; Wiemer and Wyss, 2000), the one introduced by Godano (2017), and the goodness of the fit method (GFM; Wiemer and Wyss, 2000). The last two methods always provide similar values of m_c, and we adopt for m_c the maximum of the three values (see Table 5). For all the catalogs, the m_c-values in the two classes (A and B) are very similar. We always restrict to events with magnitude larger than the largest value of m_c between the two classes.

In Figure 2, we plot $N(m)/N(m_c)$ versus m using $\overline{\zeta} = \zeta_a$, whereas the same study with $\overline{\zeta} = \zeta_m$ is presented in Figure 3. The division by $N(m_c)$ allows us to simplify the

TABLE 5
The m_c Values for the Three Different Areas Analyzed Here for the Two Different Classes and for the Three Different Methods

	Class A			Class B		
Area	MCM	GFM	God	MCM	GFM	God
Arabia	1.2	3.5	3.7	1.2	3.5	3.6
Canada–Alaska	1.2	3.4	3.5	1.2	3.5	3.5
Japan	1.8	3.0	3.0	1.8	3.0	3.0
Italy	1.4	2.2	2.2	1.8	2.1	2.2
North California	1.2	2.7	2.7	1.2	2.7	2.7
Fennoscandia	0.9	2.5	2.5	0.9	2.4	2.5
South California	1.2	2.5	2.5	1.2	2.5	2.5
United States–California	1.5	3.5	3.5	1.5	3.5	3.5
Tibet and China	1.4	3.9	4.1	1.4	3.9	4.1

The one introduced by Godano (2017), the maximum curvature method (MCM) (Wiemer and Wyss, 2000), and the goodness of the fit method (GFM) (Wiemer and Wyss, 2000).

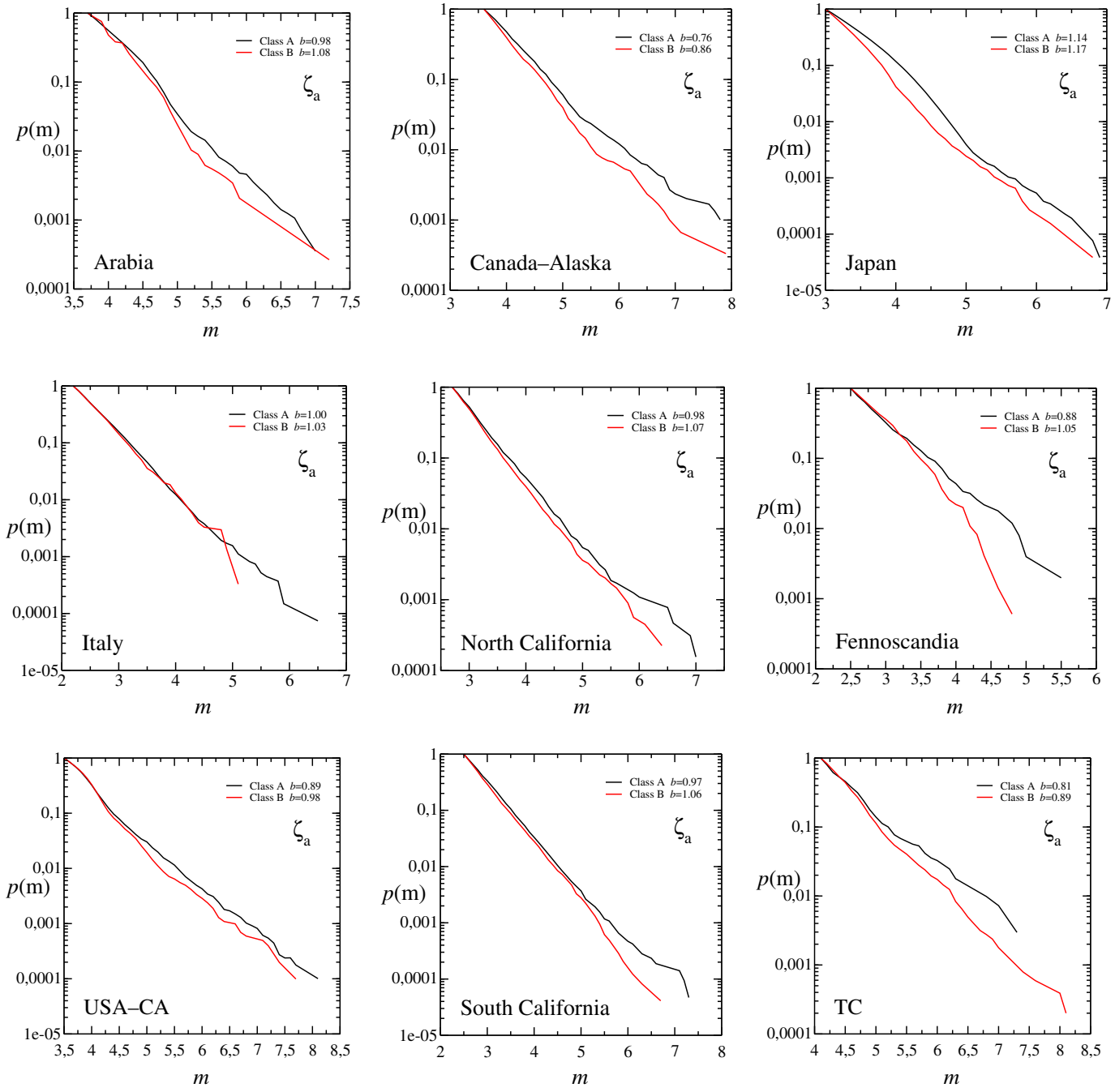

contribution of the constant a in the GR law and to better enlighten eventual differences in the b-value. Figures 2 and 3 show that, in all geographic regions, $N(m)/N(m_c)$ evaluated for event belonging to class A is always larger than the same quantity evaluated for earthquakes belonging to class B. This already suggests that the b-value in class A is smaller than in class B. To support this conclusion, we explicitly evaluate the b-values in both the classes, considering all the earthquakes with magnitude larger than a threshold magnitude m_{th}. More precisely, we use the maximum likelihood method (Aki, 1965) $b = \frac{1}{\log(10)} \frac{1}{\langle m \rangle - m_c + \Delta m}$, in which $\langle m \rangle$ is the average value of the magnitude, including only events with $m_i \geq m_{\mathrm{th}}$, and Δm is the

Figure 2. The size–frequency distribution of earthquakes occurring in regions with $\zeta_{\mathrm{min}} < \zeta < \zeta_a$ (class A) is plotted in black, whereas one of the earthquakes occurring in regions with $\zeta_a < \zeta < \zeta_{\mathrm{max}}$ (class B) is plotted in red. Different panels correspond to the different geographic areas. The number of events in class A and class B are 1451 and 5640 for Arabia; 5388 and 5730 for Canada–Alaska; 23,728 and 28,343 for Japan; 13,464 and 3034 for Italy; 6452 and 8904 for North California; 504 and 2805 for Fennoscandia; 21,317 and 24,348 for South California; 29,367 and 10,103 for United States–California; and 337 and 5064 for Tibet and China (TC), respectively. The color version of this figure is available only in the electronic edition.

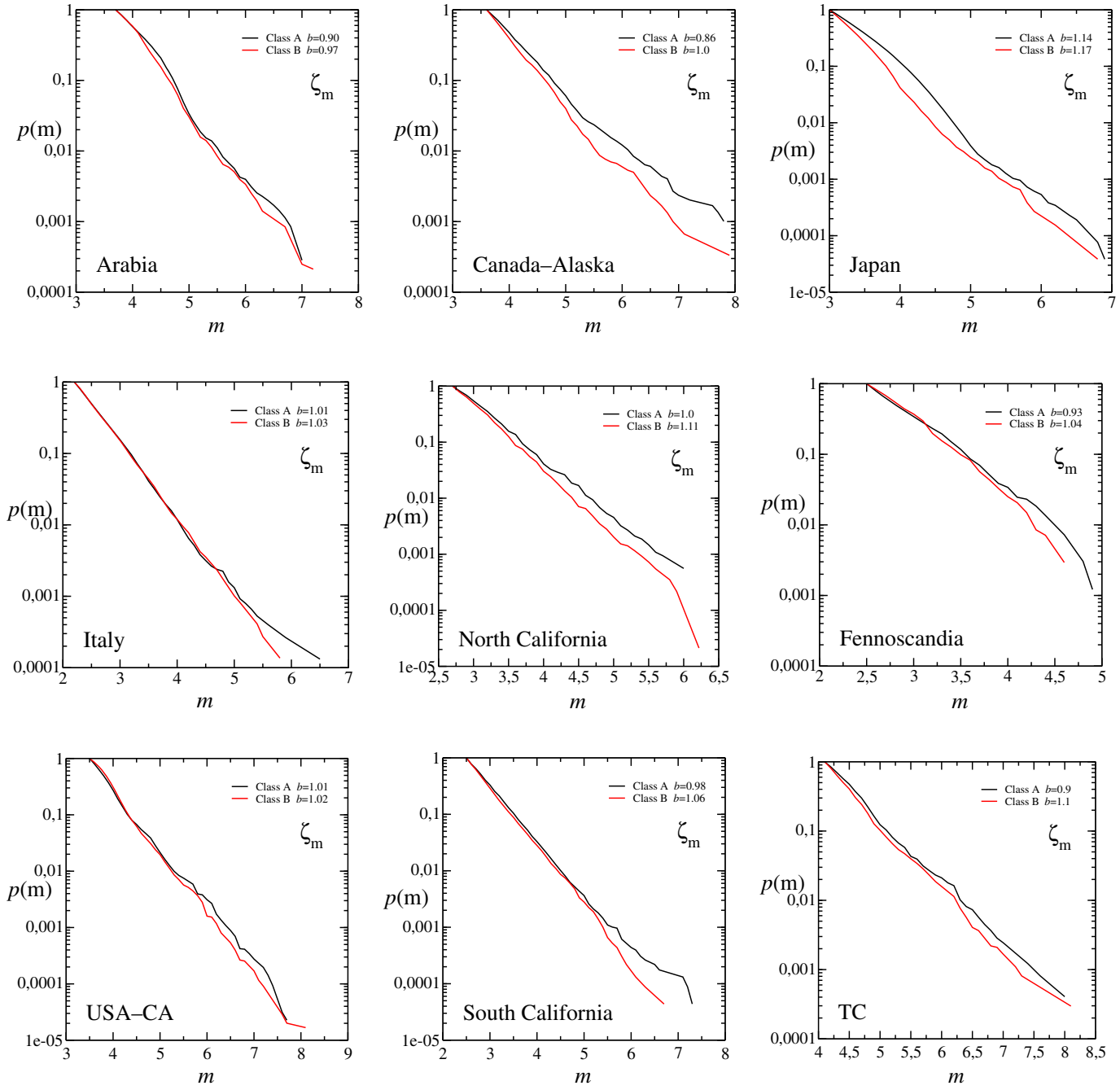

magnitude binning. The error in the b estimate σ_b has been evaluated using the Shi and Bolt (1982) method, leading to $\sigma_b = \log(10) b^2 \frac{\sigma_m}{\sqrt{N(N-1)}}$ (Shi and Bolt, 1982), in which σ_m is the standard deviation of the magnitude, and N is the number of earthquakes with $m > m_{th}$. We then define b_A as the b-value obtained for events belonging to class A and b_B as the b-value obtained for events belonging to class B. In Figure 4, we plot the values of b_A and b_B as a function of a threshold magnitude m_{th}, considering both the cases $\overline{\zeta} = \zeta_a$ and $\overline{\zeta} = \zeta_m$. Figure 4 shows that for different values of m_{th}, in all the regional catalogs and for different definitions of $\overline{\zeta}$ the condition $b_A < b_B$ appears always fullfilled.

Figure 3. The size–frequency distribution of earthquakes occurring in regions with $\zeta_{\text{min}} < \zeta < \zeta_m$ (class A) is plotted in black, whereas the one of earthquakes occurring in regions with $\zeta_m < \zeta < \zeta_{\text{max}}$ (class B) is plotted in red. Different panels correspond to the different geographic areas. The color version of this figure is available only in the electronic edition.

In Table 6 when $\overline{\zeta} = \zeta_a$ and in Table 7 when $\overline{\zeta} = \zeta_m$ we report the completeness magnitude m_c, the b-values for $m_{\text{th}} = m_c$, their standard deviation, and the number of the events used in estimating b_A and b_B. Tables 6 and 7 also report the key quantity of our study $\Delta b = b_B - b_A$, evaluated for $m_{\text{th}} = m_c$. We find that in all the cases $\Delta b > 0$, and, in

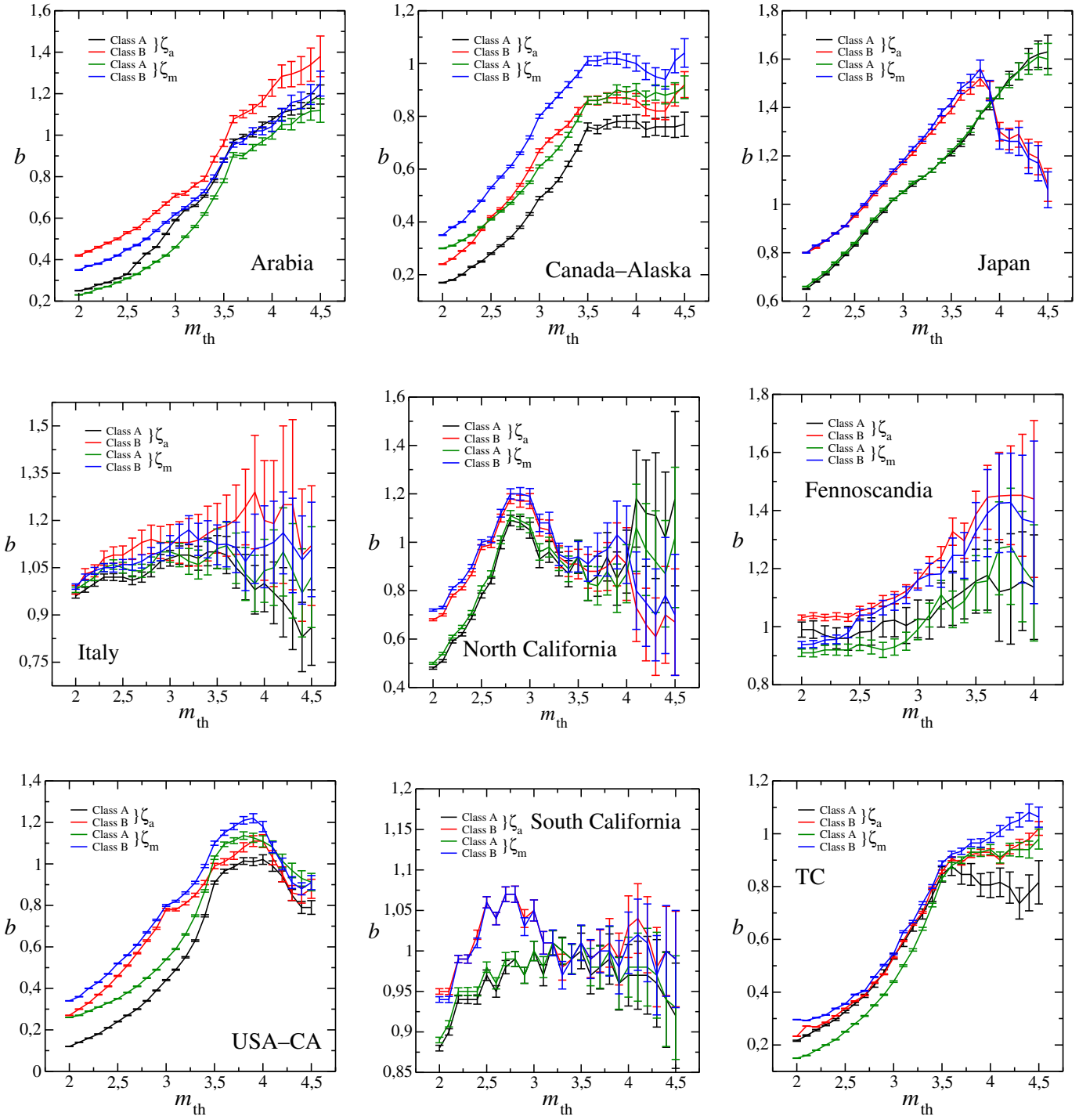

Figure 4. The *b*-values as a function of the threshold magnitude m_{th} for the different areas are analyzed here. The color version of this figure is available only in the electronic edition.

particular, for eight regions we find that $\Delta b > 2\sigma_b$, indicating that the two values of b can be considered different at the 95% of significance level. The only exceptions is represented by Italy, where Δb is still larger than zero but smaller than $2\sigma_b$.

To better validate our results and exclude that it could be obtained by chance, we compare the experimental dependence of b on ζ, considering reshuffled catalogs. They are obtained interchanging the value of ζ_i between any two randomly chosen earthquakes belonging to the same regional catalog. We restrict to earthquakes with $m_i > m_c$ and implement 10^5 independent realizations of the reshuffled catalogs. In each realization, we evaluate the difference $\Delta b_r = b_B - b_A$ and then construct the distribution $p(\Delta b_r)$, which represents the fraction of reshuffled catalogs with a given value of Δb_r. As expected, $p(\Delta b_r)$ presents a bell shape, consistent with a Gaussian distribution, centered in zero (Fig. 5). We then compare Δb_r obtained in reshuffled catalogs with the value Δb

TABLE 6
The *b*-Values, Their Standard Deviation σ_b, the Number of the Earthquakes *N* Used in the *b* Estimation, and the *b*-Value Differences Δb for the Different Areas Analyzed Here for the Two Different Classes and Using ζ_a

	Class A			Class B			
Area	b_A	σ_b	N_A	b_B	σ_b	N_B	Δb
Arabia	0.98	1.8×10^{-02}	1,451	1.08	1.1×10^{-02}	5,640	0.1
Canada–Alaska	0.76	9.2×10^{-03}	5,388	0.86	1.0×10^{-02}	5,730	0.1
Japan	1.14	5.0×10^{-03}	23,728	1.17	6.2×10^{-03}	28,343	0.03
Italy	1.00	8.3×10^{-03}	13,464	1.03	1.8×10^{-02}	3,034	0.03
North California	0.98	1.2×10^{-02}	6,452	1.07	1.1×10^{-02}	8,904	8.8×10^{-02}
Fennoscandia	0.88	4.3×10^{-02}	504	1.05	1.6×10^{-02}	2,805	0.17
South California	0.97	6.5×10^{-03}	21,317	1.06	6.8×10^{-03}	24,348	9.0×10^{-02}
United States–California	0.89	5.2×10^{-03}	29,367	0.98	8.7×10^{-03}	10,103	0.09
Tibet and China	0.81	5.1×10^{-02}	337	0.89	1.3×10^{-02}	5,064	0.08

measured in the original catalog. The percentage of reshuffled catalogs with $\Delta b_r > \Delta b$ represents an accurate estimate of the probability p that the observed value of $\Delta b > 0$ has occurred just by chance. The values of p are reported in Table 8 for both ζ_a and ζ_m. It can be seen that p is always very small, indicating that a larger b-value in regions with a larger ζ is a statistically stable result.

We have also performed the Utsu test (Utsu, 1999) to support the previous conclusion. The test provides an estimate of the probability that b_A and b_B are equal from the expression $P_{AB} = e^{-\frac{\Delta_{AB}}{2}-2}$ with:

$$\Delta_{AB} = -2(N_A + N_B)\ln(N_A + N_B) + 2N_A \ln\left(N_A + \frac{N_B b_A}{b_B}\right) + 2N_B \ln\left(N_B + \frac{N_A b_B}{b_A}\right). \quad (1)$$

This probability, both when using ζ_a and ζ_m, is smaller than 1×10^{-5} in six regions and assumes the larger, but even small, values for Italy, Fennoscandia, and Tibet and China (Table 8). In Table 8, the value equal to 0 corresponds to $p < 10^{-10}$. The test, therefore, supports our claim about the significance of the difference between b_A and b_B, even in the case of Italy.

DISCUSSION

Results presented in the previous section clearly show that the b-value in thicker areas is statistically larger than the one obtained in thinner ones. In this section, we address the possibility that our finding is an indirect consequence of the b-value dependence on the hypocentral depth and/or on the focal mechanism. More precisely, we address this issue focusing on the southern California catalog, which contains a sufficient number of earthquakes and a sufficient variability in ζ_i. This allows us to divide the $\zeta_{\max} - \zeta_{\min}$ interval in 10 classes, instead of two classes, as earlier, such as an earthquake belongs to the class A_k if $\zeta(k) < \zeta \le \zeta(k+1)$ with $k \in [1, 9]$ an $\zeta(k) = \zeta_{\min} + k(\zeta_{\max} - \zeta_{\min})/10$. More precisely, we use $\zeta_{\min} = 25$ km and $\zeta_{\max} = 40$ km, and we also consider the class A_0, which includes all the earthquakes with $\zeta \in (10, 25]$ km. We evaluate b and σ_b inside each of the A_k classes, and the results are plotted in Figure 6. We find that b rapidly changes from $b \simeq 0.6$ when $\zeta(k) = 25$ km to $b \simeq 1$

TABLE 7
The *b*-Values, Their Standard Deviation σ_b, the Number of the Earthquakes *N* Used in the *b* Estimation and the *b*-Value Differences Δb for the Different Areas Analyzed Here for the Two Different Classes and Using ζ_m

	Class A		Class B		
Area	b_A	σ_b	b_B	σ_b	Δb
Arabia	0.90	1.4×10^{-02}	0.97	1.3×10^{-02}	0.07
Canada–Alaska	0.83	1.5×10^{-02}	1.0	1.8×10^{-02}	0.17
Japan	1.14	4.8×10^{-03}	1.17	6.6×10^{-03}	0.03
Italy	1.01	1.1×10^{-02}	1.03	1.2×10^{-02}	0.02
North California	1.0	4.1×10^{-03}	1.11	4.505×10^{-03}	0.11
Fennoscandia	0.93	2.2×10^{-02}	1.04	1.9×10^{-02}	0.11
South California	0.98	6.4×10^{-02}	1.06	7.0×10^{-02}	0.08
United States–California	1.03	8.3×10^{-03}	1.1	1×10^{-02}	0.07
Tibet and China	0.90	2×10^{-02}	1.01	1.78×10^{-02}	0.11

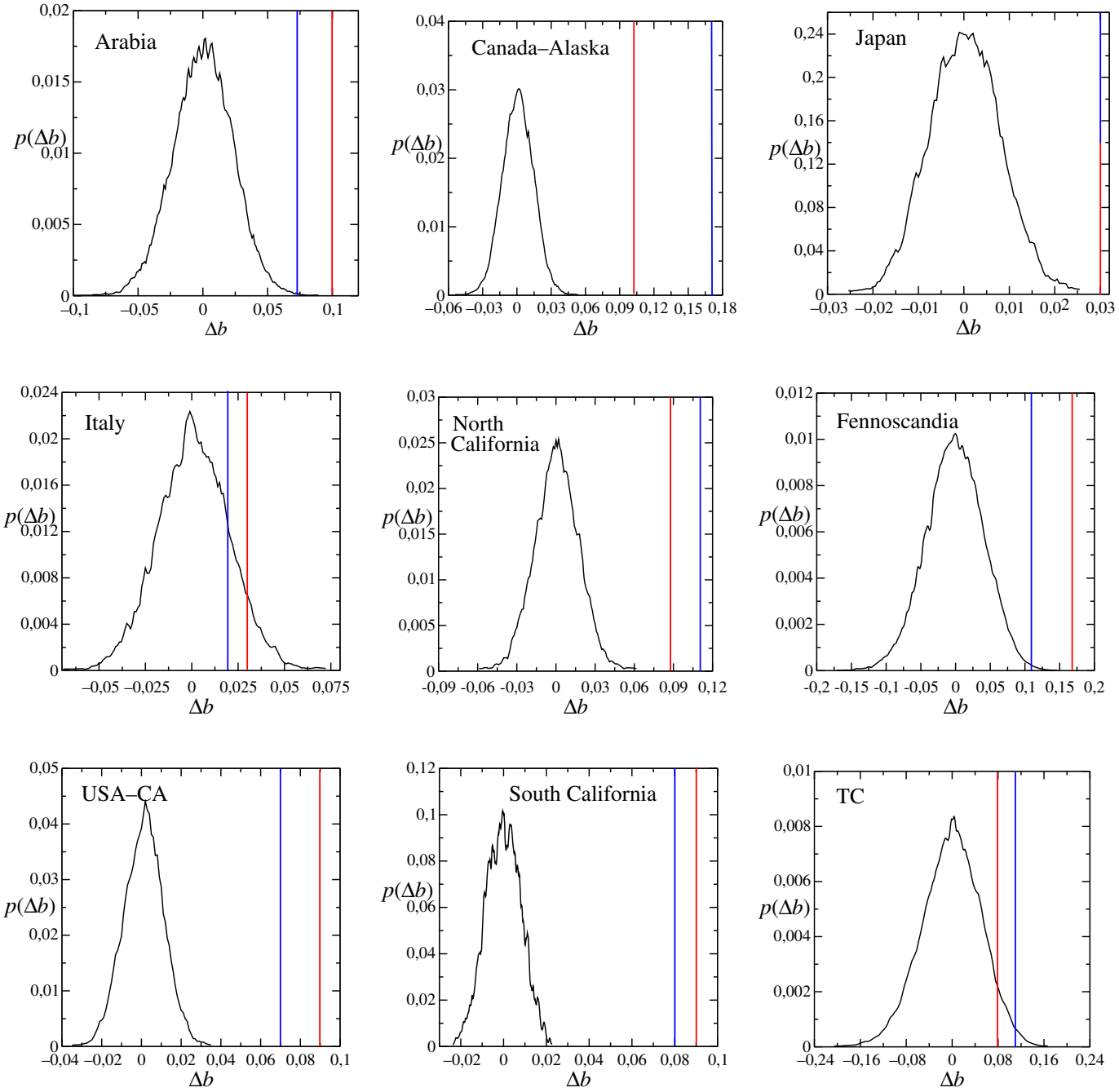

Figure 5. The distribution $p(\Delta b_r)$ obtained from the reshuffling procedure inside the nine considered regions. The vertical line, in each panel, indicates the value of Δb obtained from the regional catalog for both $\overline{\zeta} = \zeta_a$ (red) and $\overline{\zeta} = \zeta_m$ (blue). The color version of this figure is available only in the electronic edition.

when $\zeta = 30$ km. This rapid increase is responsible for a b-value in thicker regions with $\zeta_i > 30$ km significantly larger than the one in thinner regions with $\zeta_i < 30$ km.

We first remark that this result cannot be related to the dependence of the b-value on the hypocentral depth z. Several studies (Gutenberg and Richter, 1944; Eaton *et al.*, 1970; Evernden, 1970; Wyss, 1973; Mori and Abercrombie, 1997; Gerstenberger *et al.*, 2001; Spada *et al.*, 2013; Popandopoulos and Lukk, 2014; Petruccelli, Gasperini, *et al.*, 2019) have already shown that, as a consequence of the differential stress increasing with depth, the b-value decreases by increasing the hypocentral depth z_i. We have verified that this trend is observed also for the southern California catalog considered in this study. At the same time, to show that the dependence of the b-value on ζ is a novel result, not related to the dependence of the b-value on $\langle z \rangle_k$, in Figure 6a we plot $\langle z \rangle_k$ as function of $\zeta(k)$. We find that $\langle z \rangle_k$ rapidly increases in the interval $\zeta(k) \in [25, 33]$ km. In the hypothesis that b was only controlled by $\langle z \rangle_k$ and not by $\zeta(k)$, the b-value in this $\zeta(k)$ interval should decrease. Conversely, we find that b

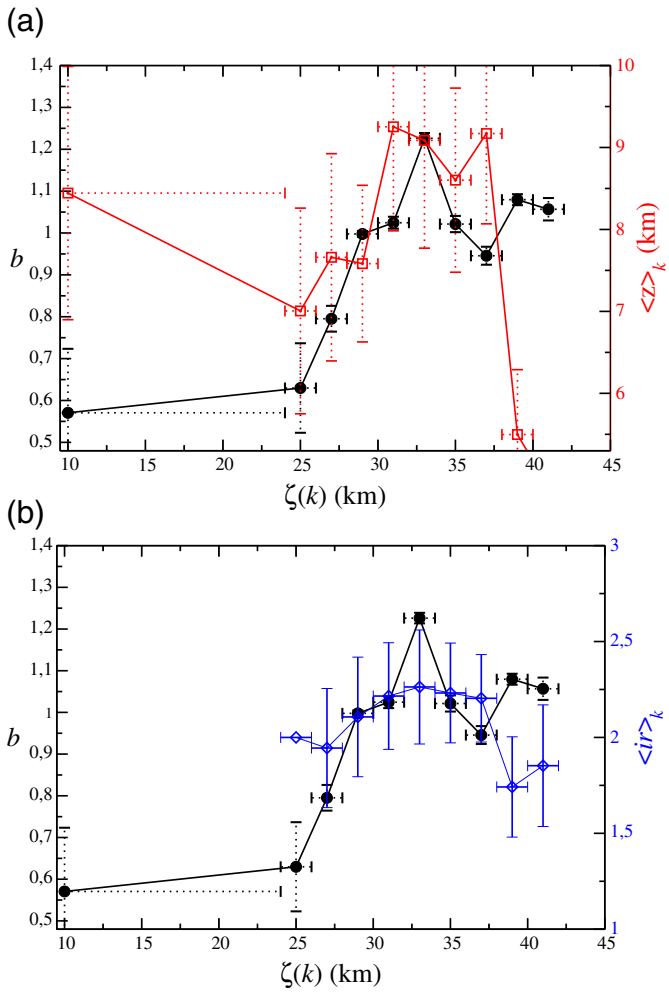

Figure 6. (a) The *b*-value (black filled circles) and the average focal depth (red empty squares) are plotted as function of the Moho depth $\zeta(k)$ for the southern California catalog. (b) The *b*-value (black filled circles) and the average rake angle $\langle ir \rangle_k$ (blue empty diamonds) are plotted as function of the Moho depth $\zeta(k)$ for the southern California catalog. Vertical error bars indicate one standard deviation, whereas horizontal bars represent the width of each class A_k. The color version of this figure is available only in the electronic edition.

rapidly increases, demonstrating that the dependence of b on $\zeta(k)$ is not related to the well-known decrease of b with the average hypocentral depth $\langle z \rangle_k$.

We next turn to explore the potential impact of different focal mechanisms on our results. The differential stress depends on the rake angle λ (Sibson, 2013), and, in particular, a larger differential stress is found for thrust faults and a smaller one for normal faults. The *b*-value is indeed found to be larger for normal faults, smaller for thrust ones, and intermediate for strike-slip faults (Schorlemmer *et al.*, 2005). In our study, we evaluate the average value of the rake angle inside each of the classes A_k, using the information contained in the catalog (Yang *et al.*, 2012) updated up to 2019 (see Table 1). We remark that this catalog contains less events than the Southern California Earthquake Data Center (SCEDC) catalog considered in previous analyses. More precisely to each earthquake in the catalog we associate and index $ir = 3$, if the rake angle $\lambda \in [45°, 135°]$, $ir = 1$ if $\lambda \in [-135°, -45°]$ and $ir = 2$ for all other λ values corresponding to strike-slip faulting. In agreement with the results of Schorlemmer *et al.* (2005), events with index $ir = 1$ exhibits a *b*-value, which is on average larger than the *b*-value for events with index $ir = 2$, which in turn is on average larger than the *b*-value for events with index $ir = 3$. Accordingly, the predominance of earthquakes belonging to a given class of faulting style leads to changes on the average value of *ir*, which is inversely correlated to a change of the *b*-value. For this reason, we evaluate the average value $\langle ir \rangle_k$ of the index *ir* inside each of the 10 A_k classes. Results are plotted in Figure 6b. The catalog (Yang *et al.*, 2012) presents no earthquake in the class A_0 corresponding to the thinnest crust. For the other classes, we do not find a clear dependence of $\langle ir \rangle_k$ on $\zeta(k)$. Only for $\zeta(k) \geq 39$ km, we find a smaller value of $\langle ir \rangle_k$, indicating a predominance of thrust faulting. This figure shows that the deviations of $\langle ir \rangle_k$ from the mean value $\langle ir \rangle \simeq 2k$ are not correlated to the observed dependence of the *b*-value on $\zeta(k)$, which, as a consequence, cannot be attributed to the predominance of a given faulting style.

TABLE 8
The Probability *p* That the Observed Value of $\Delta b > 0$ Has Occurred Just by Chance

	Reshuffled		Utsu Formula	
Area	ζ_a	ζ_m	ζ_a	ζ_m
Arabia	0	1.13×10^{-03}	5.25×10^{-04}	9.45×10^{-04}
Canada–Alaska	0	0	0	0
Japan	0	0	0	0
Italy	0.11	0.16	0.12	0.12
North California	0	0	0	0
Fennoscandia	0	2.4×10^{-03}	1.3×10^{-04}	6.6×10^{-02}
South California	0	0	0	0
United States–California	0	0	0	5.5×10^{-07}
Tibet and Chia	1.12×10^{-02}	5.4×10^{-02}	3.2×10^{-02}	3.8×10^{-05}

p has been derived by the reshuffling procedure (see Results section for details) or using the Utsu formula 1.

Excluding that our results are influenced by differences in faulting style or focal depth, we propose a new interpretation of the mechanism responsible for a smaller shear stress concentration in regions with a thinner crust. The proposed mechanisms preserves the hypothesis that the *b*-value is controlled by the local stress. More precisely, our hypothesis originates from the improvement in geodetic measurement that have pointed out the continuous slip at slow velocity of the Earth's surface, observed for a period of a year or even longer, after the majority of large earthquakes (Savage and Svarc, 1997; Burgmann *et al.*, 2002; Hsu *et al.*, 2002, 2006; Fialko, 2004; Chlieh *et al.*, 2008; Pollitz *et al.*, 2019). It has been proposed that (Perfettini and Avouac, 2004, 2007; Perfettini *et al.*, 2005, 2018, 2019; Perfettini and Ampuero, 2008) this postseismic slip, usually termed afterslip, is the main mechanism responsible for aftershock occurrence. Within this interpretation, large earthquakes produce a static stress redistribution not only within the brittle region of the crust but also within the ductile zone, at greater depth and higher temperature, triggering its creeping behavior. This region, defined as brittle creeping fault zone (BCFZ) by Perfettini and Avouac (2004), corresponds to the midcrustal fault portion where temperature gets higher than about 250°C but remains too low to activate ductile flow associated with crystal plasticity. Within this zone, brittle deformation is expected to be rate strengthening, favoring quasi-static stable shear. The induced creeping within the BCFZ transfers back the received static stress to the brittle zone, causing the occurrence of aftershocks. This mechanism implemented in numerical models for the seismic fault very well reproduces empirical laws for the occurrence of aftershocks and foreshocks (Lippiello, Petrillo, *et al.*, 2019; Petrillo *et al.*, 2020). Our hypothesis is that the brittle zone is wider in regions with a larger ζ and, therefore, taking into account that stress in the BCFZ is given back to the brittle region, we expect a higher stress concentration in regions with a smaller ζ. This hypothesis could be validated by searching for the existence of nontrivial correlations between the Moho depth and the local strain rate. At the same time, it is clearly supported by the mechanical model introduced by Petrillo *et al.* (2020), in which the seisimic fault is modeled as an elastic layer under Coulomb friction embedded in a more ductile region, modeled as a second layer subject to velocity-strengthening rheology. The coupling between the two layers is larger when the thickness of the first layer, namely the brittle one, is higher (Marone *et al.*, 1991). Interestingly, numerical catalogs present higher *b*-values for larger coupling, that is, a thicker brittle region.

CONCLUSIONS

We have shown that the *b*-value increases with the Moho depth ζ, and we have proposed a mechanism that can be responsible for the observed dependence based on two hypotheses: (1) the *b*-value is inversely proportional to the differential stress (Scholz, 1968; Amitrano, 2003), (2) the coseismic stress transferred to the midcrustal fault portion, the BCFZ zone, induces brittle creeping during the afterslip process, which, in turns, gradually gives back the received stress to the brittle region. As a consequence, for equal stress released by a large earthquake, areas with a thicker brittle region present a smaller stress concentration, which is responsible for a higher *b*-value. Our further assumption is that the thickness of the brittle region is proportional to ζ, and, therefore, a smaller ζ leads to a higher stress concentration, which is therefore responsible for a smaller *b*. The same behavior is expected also in the hypothesis that the afterslip process involves also the viscoelastic relaxation of the asthenosphere. We remark that this mechanism is not related to the mean depth of the location of the brittle region but to its thickness. This explains why the dependence of the *b*-value on the Moho depth can be the opposite of its dependence on the hypocentral depth and does not contradict previous findings.

There exist several properties of the crust, which are related to its thickness, but we have not found satisfactory arguments to explain why they could be responsible for the observed dependence of the *b*-value. For instance, geothermal properties usually depend on the crust thickness with thinner crust regions expected to be warmer than thicker ones. However, because larger values of *b* are commonly observed in regions with high temperatures, as testified by earthquakes in volcanic areas (McNutt, 2005), temperature differences should produce higher values of *b* in thinner crust zones, which is the opposite of what we observe. Nevertheless, this does not exclude that geothermal features or other mechanisms can be responsible for our findings.

In conclusion, our study shows that the Moho depth must be properly considered in all studies using the *b*-value to discriminate between zones with greater or smaller capability to accumulate stress and to nucleate the future large earthquakes. Moreover, our interpretation in terms of stress exchange between the brittle portion of the crust and the BCFZ could support the scenario where afterslip plays a central role in stress concentration, representing an experimental confirmation of the results obtained by (Lippiello, Petrillo, *et al.*, 2019; Petrillo *et al.*, 2020).

DATA AND RESOURCES

Our data are, essentially, the magnitude and the Moho depth. It is possible to find the data in ASCII format at https://zenodo.org/record/4147296#.X5l5xFhKjIV or 10.5281/zenodo.4147296. The authors would like to acknowledge the International Seismological Centre (ISC), the Japan Meteorological Agency (JMA), the Istituto Nazionale di Geofisica e Vulcanologia (INGV), the Northern California Earthquake Data Center (NCEDC), and the Southern California Earthquake Data Center (SCEDC) for providing the earthquake catalog, which can be downloaded at isc.ac.uk/iscbulletin/search/catalogue for Arabia, Canada–Alaska, Fennoscandia, United States, and Tibet and China; data.jma.go.jp/svd/eqev/data/bulletin/index_e.html for Japan; cnt.rm.ingv.it for Italy; https://ncedc.org/

ncedc/catalog-search.html for North California; scedc.caltech.edu/research-tools/altcatalogs.html for South California. All websites were last accessed in October 2020.

DECLARATION OF COMPETING INTERESTS

The authors declare that they have no conflict of interest. This research would be used only for scientific research and would not be passed on to third parties.

ACKNOWLEDGMENTS

Cataldo Godano and Anna Trameli would like to thank the Ministero dell'Istruzione, dell'Università e della Ricerca scientifica (MIUR) project PRIN 2017 WZFT2p for financial support. Cataldo Godano and Eugenio Lippiello acknowledge the support by the Program VAnviteLli pEr la RicErca: VALERE 2019, financed by the University of Campania "L. Vanvitelli." Eugenio Lippiello acknowledges support from MIUR-PRIN project "Coarse-grained description for non-equilibrium systems and transport phenomena (CO-NEST)" number 201798CZLJ.

REFERENCES

Abrehdary, M., and L. E. Sjöberg (2021). A new moho depth model for fennoscandia with special correction for the glacial isostatic effect, *Pure Appl. Geophys.* **178,** no. 3, 877–888, doi: 10.1007/s00024-021-02672-8.

Agostinetti, N. P., and A. Amato (2009). Moho depth and vp/vs ratio in peninsular Italy from teleseismic receiver functions, *J. Geophys. Res.* **114,** no. B6, doi: 10.1029/2008JB005899.

Aki, K. (1965). Maximum likelihood estimate of *b* in the formula logn = a–bm and its confidence limits, *Bull. Earthq. Res. Inst. Univ. Tokyo* **43,** 237–239.

Amitrano, D. (2003). Brittle-ductile transition and associated seismicity: Experimental and numerical studies and relationship with the b value, *J. Geophys. Res.* **108,** no. B1, 2156–2202, doi: 10.1029/2001JB000680.

Bagherbandi, K., L. E. Sjöberg, R. Tenzer, and M. Abrehdary (2015). A new fennoscandian crustal thickness model based on crust1.0 and a gravimetric-isostatic approach, *Earth Sci. Rev.* **145,** 132–145, doi: 10.1016/j.earscirev.2015.03.003.

Bannister, S. C., B. O. Ruud, and E. S. Husebye (1991). Tomographic estimates of sub-moho seismic velocities in fennoscandia and structural implications, *Tectonophysics* **189,** nos. 1/4, 37–53.

Baranov, A. A. (2010). A new crustal model for central and southern Asia, *Izv. Phys. Solid Earth* **46,** no. 1, 34–46.

Burgmann, S., S. Ergintav, P. Segall, E. H. Hearn, S. McClusky, R. E. Reilinger, H. Woith, and J. Zschau (2002). Time-dependent distributed afterslip on and deep below the izmit earthquake rupture, *Bull. Seismol. Soc. Am.* **92,** no. 1, 126–137, doi: 10.1785/0120000833.

Chlieh, M., J. P. Avouac, K. Sieh, D. H. Natawidjaja, and J. Galetzka (2008). Heterogeneous coupling of the sumatran megathrust constrained by geodetic and paleogeodetic measurements, *J. Geophys. Res.* **113,** no. B5, doi: 10.1029/2007JB004981.

de Arcangelis, L., C. Godano, and E. Lippiello (2018). The overlap of aftershock coda-waves and short-term post seismic forecasting, *J. Geophys. Res.* **123,** no. 7, 5661–5674, doi: 10.1029/2018JB015518.

Di Giacomo, D., and D. A. Storchak (2016). A scheme to set preferred magnitudes in the ISC bulletin, *J. Seismol.* **20,** no. 2, 555–567, doi: 10.1007/s10950-015-9543-7.

Eaton, J. P., M. E. O'Neill, and J. N. Murdock (1970). Aftershocks of the 1966 Parkfield-Cholame, California, earthquake: A detailed study*, *Bull. Seismol. Soc. Am.* **60,** no. 4, 1151–1197.

Enescu, B., J. Mori, and M. Miyazawa (2007). Quantifying early aftershock activity of the 2004 mid-niigata prefecture earthquake (mw6.6), *J. Geophys. Res.* **112,** no. B4, doi: 10.1029/2006JB004629.

GIS (2011). Arcgis desktop: Release 10, 2011, available at https://www.esri.com/en-us/home (last accessed December 2020).

Evernden, J. F. (1970). Study of regional seismicity and associated problems, *Bull. Seismol. Soc. Am.* **60,** no. 2, 393–446.

Fialko, Y. (2004). Probing the mechanical properties of seismically active crust with space geodesy: Study of the coseismic deformation due to the 1992 mw7.3 landers (southern california) earthquake, *J. Geophys. Res.* **109,** no. B3, doi: 10.1029/2003JB002756.

Gerstenberger, M., S. Wiemer, and D. Giardini (2001). A systematic test of the hypothesis that the b value varies with depth in california, *Geophys. Res. Lett.* **28,** no. 1, 57–60, doi: 10.1029/2000GL012026.

Godano, C. (2017). A new method for the estimation of the completeness magnitude, *Phys. Earth Planet. In.* **263,** 7–11, doi: 10.1016/j.pepi.2016.12.003.

Gulia, L., and S. Wiemer (2010). The influence of tectonic regimes on the earthquake size distribution: A case study for Italy, *Geophys. Res. Lett.* **37,** no. 10, doi: 10.1029/2010GL043066.

Gutenberg, B., and C. F. Richter (1944). Frequency of earthquakes in California, *Bull. Seismol. Soc. Am.* **34,** 185–188.

Hainzl, S. (2016a). Apparent triggering function of aftershocks resulting from rate–dependent incompleteness of earthquake catalogs, *J. Geophys. Res.* **121,** no. 9, 6499–6509, doi: 10.1002/2016JB013319.

Hainzl, S. (2016b). Rate-dependent incompleteness of earthquake catalogs, *Seismol. Res. Lett.* **87,** no. 2A, 337–344.

Hauksson, E., P. Shearer, and W. Yang (2012). Waveform relocated earthquake catalog for southern california (1981 to june 2011), *Bull. Seismol. Soc. Am.* **102,** no. 5, 2239–2244, doi: 10.1785/0120120010.

Helmstetter, A., Y. Y. Kagan, and D. D. Jackson (2006). Comparison of short-term and time-independent earthquake forecast models for southern California, *Bull. Seismol. Soc. Am.* **96,** no. 1, 90–106, doi: 10.1785/0120050067.

Herrmann, M., and W. Marzocchi (2021). Inconsistencies and lurking pitfalls in the magnitudefrequency distribution of high-resolution earthquake catalogs, *Seismol. Res. Lett.* **92,** no. 2A, doi: 10.1785/0220200337.

Hsu, Y., N. Bechor, P. Segall, S. B. Yu, L. C. Kuo, and K. F. Ma (2002). Rapid afterslip following the 1999 Chi-Chi, Taiwan earthquake, *Geophys. Res. Lett.* **29,** no. 16, doi: 10.1029/2002GL014967.

Hsu, Y. J., M. Simons, J. P. Avouac, J. Galetzka, K. Sieh, M. Chlieh, D. Natawidjaja, L. Prawirodirdjo, and Y. Bock (2006). Frictional afterslip following the 2005 Nias-Simeulue earthquake, Sumatra, *Science* **312,** no. 5782, 1921–19266.

Kagan, Y. Y. (2004). Short-term properties of earthquake catalogs and models of earthquake source, *Bull. Seismol. Soc. Am.* **94,** no. 4, 1207–1228.

Kamer, Y., and S. Hiemer (2015). Data-driven spatial b value estimation with applications to california seismicity: To b or not to b, *J. Geophys. Res.* **120,** no. 7, 5191–5214, doi: 10.1002/2014JB011510.

Kanamori, H. (1983). Magnitude scale and quantification of earthquakes, *Tectonophysics* **93,** nos. 3/4, doi: 10.1016/0040-1951(83)90273-1.

Katsumata, A. (2010). Depth of the Moho discontinuity beneath the Japanese Islands estimated by traveltime analysis, *J. Geophys. Res.* **115,** no. B4, doi: 10.1029/2008JB005864.

Lippiello, E., A. Cirillo, C. Godano, E. Papadimitriou, and V. Karakostas (2019). Post seismic catalog incompleteness and aftershock forecasting, *Geosciences* **9,** no. 8, 355, doi: 10.3390/geosciences9080355.

Lippiello, E., F. Giacco, W. Marzocchi, C. Godano, and L. de Arcangelis (2017). Statistical features of foreshocks in instrumental and ETAS catalogs, *Pure Appl. Geophys.* **174,** no. 4, 1679–1697, doi: 10.1007/s00024-017-1502-5.

Lippiello, E., C. Godano, and L. de Arcangelis (2019). The relevance of foreshocks in earthquake triggering: A statistical study, *Entropy* **21,** no. 2, doi: 10.3390/e21020173.

Lippiello, E., G. Petrillo, F. Landes, and A. Rosso (2019). Fault heterogeneity and the connection between aftershocks and afterslip, *Bull. Seismol. Soc. Am.* **109,** no. 3, 1156–1163, doi: 10.1785/0120180244.

Marone, C. J., C. H. Scholtz, and R. Bilham (1991). On the mechanics of earthquake afterslip, *J. Geophys. Res.* **96,** no. B5, 8441–8452, doi: 10.1029/91JB00275.

McNutt, S. R. (2005). Volcanic seismology, *Annu. Rev. Earth planet. Sci.* **32,** 461–491.

Mooney, W. D., and M. K. Kaban (2010). The north american upper mantle: Density, composition, and evolution, *J. Geophys. Res.* **115,** no. B12, doi: 10.1029/2010JB000866.

Mori, J., and R. E. Abercrombie (1997). Depth dependence of earthquake frequency-magnitude distributions in California: Implications for rupture initiation, *J. Geophys. Res.* **102,** no. B7, 15,081–15,090, doi: 10.1029/97JB01356.

Peng, Z., J. E. Vidale, M. Ishii, and A. Helmstetter (2007). Seismicity rate immediately before and after main shock rupture from high-frequency waveforms in Japan, *J. Geophys. Res.* **112,** no. B3, doi: 10.1029/2006JB004386.

Perfettini, H., and J. P. Ampuero (2008). Dynamics of a velocity strengthening fault region: Implications for slow earthquakes and postseismic slip, *J. Geophys. Res.* **113,** no. B9, doi: 10.1029/2007JB005398.

Perfettini, H., and J.-P. Avouac (2004). Postseismic relaxation driven by brittle creep: A possible mechanism to reconcile geodetic measurements and the decay rate of aftershocks, application to the chi-chi earthquake, Taiwan, *J. Geophys. Res.* **109,** no. B2, doi: 10.1029/2003JB002488.

Perfettini, H., and J.-P. Avouac (2007). Modeling afterslip and aftershocks following the 1992 landers earthquake, *J. Geophys. Res.* **112,** no. B7, doi: 10.1029/2006JB004399.

Perfettini, H., J.-P. Avouac, and J.-C. Ruegg (2005). Geodetic displacements and aftershocks following the 2001 mw = 8.4 peru earthquake: Implications for the mechanics of the earthquake cycle along subduction zones, *J. Geophys. Res.* **110,** no. B9, doi: 10.1029/2004JB003522.

Perfettini, H., W. B. Frank, D. Marsan, and M. Bouchon (2018). A model of aftershock migration driven by afterslip, *Geophys. Res. Lett.* **45,** no. 5, 2283–2293, doi: 10.1002/2017GL076287.

Perfettini, H., W. B. Frank, D. Marsan, and M. Bouchon (2019). Updip and along-strike aftershock migration model driven by afterslip: Application to the 2011 Tohoku-Oki aftershock sequence, *J. Geophys. Res.* **124,** no. 3, 2653–2669, doi: 10.1029/2018JB016490.

Petrillo, G., F. Landes, E. Lippiello, and A. Rosso (2020). The influence of the brittle-ductile transition zone on aftershock and foreshock occurrence, *Nat. Commun.* **11,** 1–10.

Petruccelli, A., P. Gasperini, T. Tormann, D. Schorlemmer, A. P. Rinaldi, G. Vannucci, and S. Wiemer (2019). Simultaneous dependence of the earthquake-size distribution on faulting style and depth, *Geophys. Res. Lett.* **46,** no. 20, 11,044–11,053, doi: 10.1029/2019GL083997.

Petruccelli, A., D. Schorlemmer, T. Tormann, A. P. Rinaldi, S. Wiemer, P. Gasperini, and G. Vannucci (2019). The influence of faulting style on the size-distribution of global earthquakes, *Earth Planet. Sci. Lett.* **527,** doi: 10.1016/j.epsl.2019.115791.

Petruccelli, A., G. Vannucci, B. Lolli, and P. Gasperini (2018). Harmonic fluctuation of the slope of the frequency–magnitude distribution (b-Value) as a Function of the angle of Rake, *Bull. Seismol. Soc. Am.* **108,** no 4, 1864–1876, doi: 10.1785/0120170328.

Pollitz, F. F., J. R. Murray, S. E. Minson, C. W. Wicks, J. L. Svarc, and B. A. Brooks (2019). Coseismic slip and early afterslip of the m6.0 24 august 2014 south Napa, California, earthquake, *J. Geophys. Res.* **124,** no. 11, 11,728–11,747, doi: 10.1029/2019JB018470.

Popandopoulos, G. A., and A. A. Lukk (2014). The depth variations in the b-value of frequency-magnitude distribution of the earthquakes in the Garm region of Tajikistan, *Izv. Phys. Solid Earth* **50,** no. 2, 273–288.

Savage, J. C., and J. L. Svarc (1997). Postseismic deformation associated with the 1992 m_w=7.3 landers earthquake, southern California, *J. Geophys. Res.* **102,** no. B4, 7565–7577, doi: 10.1029/97JB00210.

Scholz, C. H. (1968). The frequency-magnitude relation of microfracturing in rock and its relation to earthquakes, *Bull. seism. Soc. Am.* **58,** 399–415.

Scholz, C. H. (2015). On the stress dependence of the earthquake b value, *Geophys. Res. Lett.* **42,** no. 5, 1399–1402, doi: 10.1002/2014GL062863.

Schorlemmer, D., S. Wiemer, and M. Wyss (2005). Variations in earthquake-size distribution across different stress regimes, *Nature* **437,** 539–542.

Shi, Y., and B. A. Bolt (1982). The standard error of the magnitude-frequency b value, *Bull. Seismol. Soc. Am.* **72,** no. 5, 1677–1687.

Sibson, R. H. (2013). Frictional constraints on thrust, wrench and normal faults, *Nature* **249,** 542–544.

Spada, M., T. Tormann, S. Wiemer, and B. Enescu (2013). Generic dependence of the frequency-size distribution of earthquakes on depth and its relation to the strength profile of the crust, *Geophys. Res. Lett.* **40,** no. 4, 709–714, doi: 10.1029/2012GL054198.

Storchak, D. A., J. Harris, L. Brown, K. Lieser, B. Shumba, R. Verney, and D. Di Giacomo (2020). Rebuild of the bulletin of the international seismological centre (ISC), part 2: 1980–2010, *Geosci. Lett.* **7,** no. 1, doi: 10.1186/s40562-020-00164-6.

Storchak, D. A., J. Harris, L. Brown, K. Lieser, B. Shumba, R. Verney, D. Di Giacomo, and E. I. M. Korger (2017). Rebuild of the bulletin of the international seismological centre (ISC), part 1: 1964–1979, *Geosci. Lett.* **4,** no. 1, 32, doi: 10.1186/s405620170098z.

Szwillus, W., J. C. Afonso, J. Ebbing, and W. D. Mooney (2019). Global crustal thickness and velocity structure from geostatistical

analysis of seismic data, *J. Geophys. Res.* **124,** no. 2, 1626–1652, doi: 10.1029/2018JB016593.

Thormann, T., S. Wiemer, and E. Hauksson (2010). Changes of reporting rates in the southern Californian earthquake catalog, introduced by a new definition of ml, *Bull. Seismol. Soc. Am.* **100,** no. 4, 1733–1742, doi: 10.1785/0120090124.

Utsu, T. (1999). Representation and analysis of the earthquake size distribution: A historical review and some new approaches, *Pure Appl. Geophys.* **155,** nos. 2/4, 509–535, doi: 10.1007/s000240050276.

Wiemer, S., and M. Wyss (2000). Minimum magnitude of completeness in earthquake catalogs: Examples from Alaska, the western United States, and Japan, *Bull. Seismol. Soc. Am.* **90,** no. 4, 859–869, doi: 10.1785/0119990114.

Wyss, M. (1973). Towards a physical understanding of the earthquake frequency distribution, *Geophys. J. Roy. Astron. Soc.* **31,** no. 4, 341–359, doi: 10.1111/j.1365-246X.1973.tb06506.x.

Yang, W., E. Hauksson, and P. Shearer (2012). Computing a large refined catalog of focal mechanisms for southern California (1981 2010): Temporal stability of the style of faulting, *Bull. Seismol. Soc. Am.* **12,** 1179–1194, doi: 10.1785/0120110311.

Manuscript received 26 May 2021
Published online 14 April 2022